Diffraction from a Truncated Grounded Dielectric Slab: A Comparative Full-Wave/Physical-Optics Analysis

Stefano Maci, *Senior Member, IEEE*, Leonardo Borselli, *Member, IEEE*, and Andrea Cucurachi

***Abstract*—The problem of diffraction at the edge of a semi-infinite grounded dielectric slab excited by a line source is investigated. This canonical problem may be used as a reference solution in the high-frequency regime for patch antennas radiating from a finite grounded slab. Both physical optics (PO) and integral equation (IE) approaches are used and compared. The PO formulation is cast in a convenient asymptotic form that neatly describes the diffraction processes associated with the various wave species. The IE, solved by the method of moments, is formulated by enforcing the continuity of the electric field on an infinite aperture orthogonal to the slab. This allows a drastic reduction of unknowns, provided that appropriate entire domain basis functions are used that are shaped to match the asymptotic behavior of the aperture field. Comparison between the PO and IE solutions is presented to determine the range of validity of PO.**

***Index Terms*—Dielectric slabs, electromagnetic diffraction, physical optics.**

I. Introduction

THE description of diffraction mechanisms at the edges of a grounded dielectric slab is important in practical antenna and scattering problems, in particular for the prediction of pattern distortion for patch antennas on finite substrates [1]–[3]. The typical values of thicknesses and dielectric constants used in these antennas suggest the effective use of a physical optics (PO) approximation. For the present problem, PO means that the dielectric polarization currents and the surface ground plane currents pertinent to the truncated structure are estimated like those produced in the infinite grounded slab by the actual source. Although this approach of PO for grounded slab configurations does not account for the guided wave reflection at the open end and the fringe deformation of the currents close to the edge, it contains the basic physical information for neatly describing the various wave diffraction phenomena. For certain aspects PO seems to be more adequate with respect to alternative formulations, i.e., those based on the exact solutions of wedges with impedance boundary conditions (IBC) [4], [5] or generalized impedance boundary conditions (GIBC) [6]. The solutions derived from the GIBC, although more general and complete than those from IBC, equally fail for increasing substrate thicknesses and decreasing dielectric constants (i.e., for the case of patch antenna). In general, approximate BC's cause errors in estimating the propagation constant of surface waves (SW's) and, when included in the description, of leaky waves (LW's). Furthermore, for source placed in proximity of the surface or near to the edges, the applicability of approximate BC's is questionable also for thin substrates, because they intrinsically assume a local plane wave as incident field, thus leading to possible inaccuracy in predicting the SW excitation coefficients. Although PO is lacking in the fringe field description, it does not suffer from the above limitations, being based on the exact Green's function of the infinite dielectric slab.

The application of PO to grounded slab structures was first introduced in [3] for patch antenna problems, where the calculation of both the PO current and its radiation integral was performed numerically. In [7], a PO high-frequency formulation is applied to the case of an electric dipole placed at the interface of a truncated semi-infinite grounded dielectric slab. The same formulation was applied in [8] to find the radiation pattern of patch antennas on a finite ground plane. There, via comparison with experimental data, the effectiveness of the PO approach was verified for certain substrate thicknesses and dielectric constants, but no investigation on the range of validity of PO was presented. This investigation is the main purpose of this paper.

In order to isolate the diffraction phenomena relevant to only one truncation, a canonical configuration has been chosen, which consists of a semi-infinite grounded dielectric slab excited by a line source placed at the dielectric/air interface. This problem is studied here first by an asymptotic PO formulation and next, for comparison, by a full-wave integral equation analysis. Note that the full-wave analysis for the present problem cannot be easily carried out by the conventional surface/volume formulations of the electric field integral equation like that presented in [9] for the analysis of printed antennas on finite substrate, owing to the large number of unknowns imposed by the semi-infinite extension of the integration domain. Consequently, a different and rather unconventional full-wave method is suggested in this paper, which is based on deriving the integral equation by enforcing the continuity of the tangent electric field on an infinite aperture orthogonal to the slab. Semi-infinite domain basis functions are used to expand the unknown aperture field that are shaped according to the asymptotic behavior of the field diffracted at the edge.

In order to show the kind of contributions that are not predicted by PO so as to simplify the interpretation of the comparative results presented herein after, the next section is devoted to a qualitative description of the rays involved in the excitation and diffraction mechanisms.

Manuscript received June 8, 1998.

The authors are with the Department of Information Engineering, University of Siena, 53100 Siena, Italy.

Publisher Item Identifier S 0018-926X(00)01277-1.

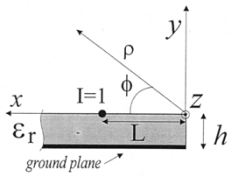

Fig. 1. Geometry of the truncated grounded dielectric slab illuminated by a line source.

II. Ray Description

The geometry we are dealing with is shown in Fig. 1, and consists of a semi-infinite grounded dielectric slab with dielectric constant ϵ_r and thickness h, which is fed by a line electric source with unit current, located at the air-dielectric interface, at a distance L from the upper edge of the truncation. A rectangular coordinate system (x, y, z) and its relevant cylindrical one (ρ, ϕ) are introduced, with their origin at the upper edge. The y axis is perpendicular to the interface, the x axis is along the interface, and the z axis is along the upper edge of the truncation. Fig. 2 is a schematic presentation of the ray contributions involved in the excitation and diffraction of various wave species.

A. Space Wave and Relevant Diffracted Rays

The GO rays are those excited by the slab-modulated source field in absence of truncation [Fig. 2(a)]. For slab problems, the summation of the GO ray contributions in the external region is often referred to as *space wave* to distinguish it from surface and leaky waves. The GO rays include the incident ray and the rays incoherently reflected between the dielectric interface and the ground plane. These rays may be attributed to direct contributions from an infinite series of image sources vertically aligned into a homogeneous dielectric half-space [10]. (Note that these sources cannot be rigorously interpreted as line electric currents, but the above interpretation help the physical understanding.) The rays launched by the source and its images with an incidence angle θ_i less than the critical angle $\theta_{\rm cr} = \sin^{-1}(1/\sqrt{\epsilon_r})$ [Fig. 2(a)] penetrate into the free-space and contribute to the space wave. The multiple reflected rays exactly incident at $\theta_{\rm cr}$ [only one of them is depicted in Fig. 2(a)] propagate in the free-space region at grazing aspect with the speed of light. The total summation of these grazing rays provides a total grazing field of asymptotic order $1/x\sqrt{x}$, thus obtaining a field that is not purely optical in its asymptotic regime. [Conditions may be found for TM case [11] in which the decay of this space wave grazing field is of $1/x^3\sqrt{x}$ type, x^{-4} for the three-dimensional case]. The asymptotic $1/x\sqrt{x}$-behavior at grazing aspect leads to a rapid variation of the field in the direction normal to the interface, thus producing a significant slope-diffraction effects at the slab truncation. Fig. 2(a) depicts the diffracted rays excited by the grazing space wave, longer arrows denoting stronger ray amplitudes. The PO approach correctly describe this behavior since it is based on the exact grounded slab Green's function. In the far-field regime, the diffracted rays provide continuity to the space-wave derivative when the observation point crosses the plane $\phi = \pi$ and allow for the illumination of the region below the ground plane. Additional diffracted rays, excited by

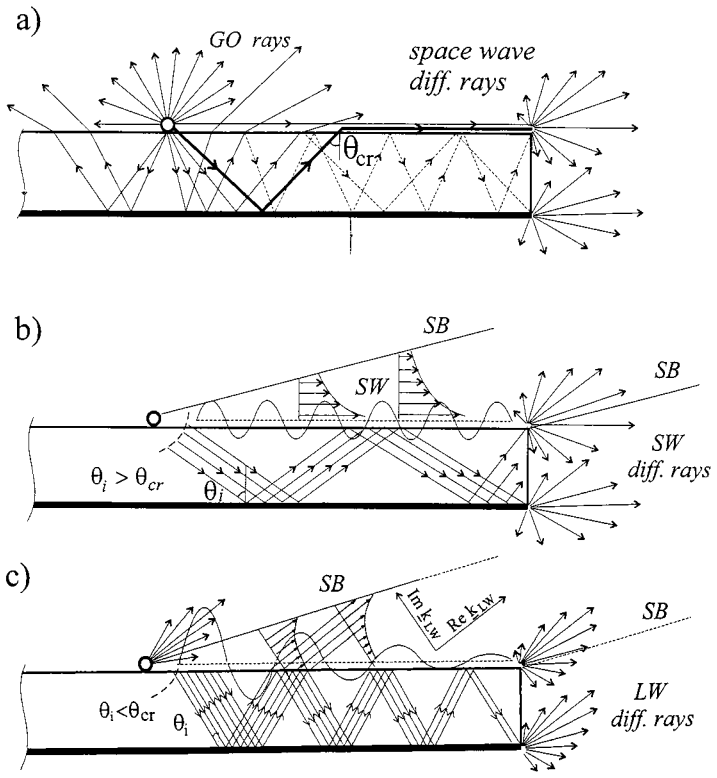

Fig. 2. Diffracted ray contributions. Ray description of excitation and diffraction mechanisms for various wave species. Longer arrows denote stronger ray amplitudes. (a) Space wave (GO rays) and relevant diffracted rays. (b) Surface wave and relevant diffracted rays (parallel arrows inside the dielectric denote a homogeneous plane wave propagating by successive relections with incidence angle greater than the critical angle. (c) Leaky wave and relevant diffracted rays (decreasing number of parallel arrows inside the dielectric denote an inhomogeneous plane wave propagating by successive reflections; the incidence angle of the real part of the vector wavenumber is less than the critical angle).

the internal GO rays, arise from the lower edge of the truncation. An approximation of this latter contribution is provided by the PO approach. Conversely, PO does not describe: a) multiple diffraction mechanisms between the two edges and b) the GO rays excited back into the slab.

B. Surface Waves and Relevant Diffracted Rays

The GO rays which impinge with $\theta_i > \theta_{\rm cr}$ may encounter—starting from a certain cutoff frequency—a condition for which the various transmitted y-evanescent grazing rays superimpose coherently in the x-direction. This creates in the external region a total y-evanescent wave which does not attenuate along x [surface wave (SW)]. Because the SW is attenuated in y, to satisfy the wave equation it travels along x with phase velocity lower than the free-space speed of light. In the slab-region, the SW can be seen as a homogeneous plane wave which undergoes successive subcritical $(\theta_i > \theta_{\rm cr})$ reflections (Fig. 2(b)). In the free-space region, the SW exists below a shadow boundary (SB) that starts at the source (when this latter is placed *on* the slab). In a uniform asymptotic analysis, the space wave excited by the source must have there an opposite discontinuity to compensate for that of the SW at the SB. At the truncation, the SW produces diffracted rays

at both the lower and the upper edge, which exhibit stronger amplitude near the paraxial ($\phi = \pi$) direction. In the near zone of observation, the SW exhibits a second SB arising from the upper edge, parallel to the previous one. The compensation of the SW discontinuity at this second SB is provided by the SW-induced diffracted-wave in a way similar at all to that mentioned for the space wave.

Due to the evanescence of the SW, its discontinuity at both SB's asymptotically vanishes. Thus, both the space wave and the SW-induced diffracted wave have to be discontinuous only in transition regions of finite extension localized close to the source and close to the edge, respectively. Therefore, in the far zone both the space wave and the SW-induced diffracted wave exhibit a regular behavior (i.e., they do not have either discontinuity nor singularity). We note that the space-wave excited diffracted rays may have discontinuity versus frequency. Indeed, the SW-excited diffracted rays appear in the far zone only for frequencies higher than the cutoff frequency of the pertinent SW. In a frequency scan, this may produce an unphysical discontinuity of the relevant diffracted ray contributions. The desired uniform description of these rays is provided by the space-wave excited diffracted rays [Fig. 2(a)], which exhibits an appropriate frequency transition close to cutoff. This phenomenon is well described by the asymptotic PO solution presented in Section III. Note that the diffracted rays can also excite reflected SW's, which are not depicted in Fig. 2(b) and are not described by PO.

C. Leaky Wave and Relevant Diffracted Rays

A coherence condition can also occur for a *inhomogeneous* plane wave, which reflects inside the dielectric with $\theta_i < \theta_{\rm cr}$. In the external region, the continuity of the tangential field is ensured by an inhomogeneous plane wave [leaky wave (LW)], which grows up along positive y [Fig. 2(c)]. The existance region of LW is restricted in the space below an SB, where it exhibits attenuation mooving away from the source. The source-excited space wave provides there the compensation of its field discontinuity. The LW propagates along x with a phase velocity greater then the speed of light, while exhibiting an exponential x attenuation. The subsequent diffraction mechanism provides then a weak field contribution compared with the one associated to space wave or SW's. An exception is when the dielectric support is properly stratified in order to enhance the LW propagation phenomenon [12]. The LW-induced diffraction mechanism can be described in a PO framework and it will be included for completeness in our asymptotic formulation, even though the LW diffraction effect is often negligible in the case of a single dielectric layer.

III. PO Formulation

By invoking the equivalence principle, the dielectric and the ground plane are replaced by polarization (volumetric) currents and conductive (surface) currents, respectively. By resorting to the PO approximation, these currents $j_z^{\rm PO}(x,y)$ may be estimated from those of the corresponding infinite grounded dielectric slab and may be expressed by the spectral Fourier representation $J_z^{\rm PO}(\kappa_x, y)\exp(-jk\kappa_x L)$ (see Appendix A) where k is

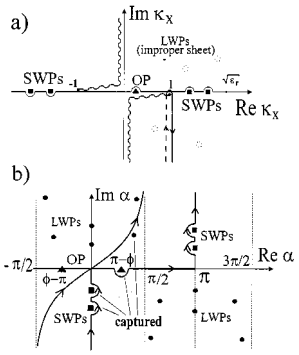

Fig. 3. (a) Complex k_x-plane. (b) Complex α-plane.

the free-space wavenumber and κ_x is the k-normalized spectral wavenumber (the time dependence $\exp(j\omega t)$ has been assumed and suppressed). The electric-z field $E_z(\rho,\phi)$ radiated at large distance is provided by the radiation integral of $j_z^{\rm PO}$ on the semi-infinite extent $x \geq 0$, i.e.,

$$E_z(\rho,\phi) = -k\zeta\sqrt{j}\frac{e^{-jk\rho}}{2\sqrt{2\pi k\rho}}(a(\phi) + e^{jkL\cos\phi}) \qquad (1)$$

where

$$a(\phi) = \int_{-h}^{0}\int_{0}^{\infty} j_z^{\rm PO}(x,y)e^{jk(x\cos\phi + y\sin\phi)}\,dx\,dy. \qquad (2)$$

Note that the second term in (1) represents the direct contribution from the unit source. Using the same method as in [7], the integral in (2) may be rewritten as

$$a(\phi) = \frac{1}{2\pi j}\int_{-\infty}^{\infty}\frac{-J(\kappa_x,\phi)}{(\kappa_x + \cos\phi)}e^{-jkL\kappa_x}d\kappa_x \qquad (3)$$

where $J(\kappa_x,\phi) = \int_{-h}^{0} J_z^{\rm PO}(\kappa_x, y)\exp(jky\sin\phi)dy$. The integral in (3) can be seen as a spectral convolution calculated at $\kappa_x' = -\cos\phi$ between the Fourier transform of the PO currents (this latter preconditioned by the integration in y) and the Fourier transform $1/j\kappa_x$ of a unit spatial-step function that provides the PO windowing of the radiation integral. The integrand in (3) exhibits a pole at $\kappa_x = -\cos\phi$ (optical pole, OP) detoured clockwise by the integration path. Fig. 3(a) shows the complex κ_x-plane. The branch-cut associated to $\kappa_x = \pm 1$ is chosen in such a way that $\mathrm{Im}(\sqrt{1-\kappa_x^2}) < 0$ on the top Riemann sheet; the integration contour in (3) detours the branch points −1 and +1 in counterclockwise and clockwise sense, respectively. Similarly, surface-wave poles (SWP's) $\kappa_{xn}^{\rm SW}(n = 1,2\cdots)$ are located on the real axis, where $\kappa_{xn}^{\rm SW}$ is the k-normalized propagation constants of the nth SW excited in the infinite dielectric slab. The integration poles are detoured in either the counterclockwise or the clockwise sense, respectively [Fig. 2(a)]; they are located on the intervals $(-1, -\sqrt{\epsilon_r})$ or $(1, \sqrt{\epsilon_r})$, which implies SW phase velocities between the speed of light in free-space and in the dielectric. The complex solutions of the dispersion equation [leaky-wave poles (LWP)] $\kappa_{xm}^{\rm LW}, m = 1,2\cdots)$ are located on the improper Riemann sheet $(\mathrm{Im}(\sqrt{1-\kappa_x^2}) > 0)$.

A steepest descent path (SDP) deformation is applied next (Section III-A) to obtain a ray representation of (3); the SDP

integration is evaluated asymptotically for large values of kL (Section III-B) to obtain a closed-form solution.

A. Space-Wave and Diffracted-Wave Contributions

It is convenient to introduce the change of variable $\kappa_x = \cos\alpha$ with $\sqrt{1-\kappa_x^2} = \sin\alpha$ so that (3) becomes

$$a(\phi) = \frac{1}{2\pi j}\int_{C_\alpha} A(\alpha) e^{-jkL\cos\alpha}\, d\alpha \tag{4}$$

in which $A(\alpha) = -(J(\cos\alpha,\phi)\sin\alpha)/(\cos\alpha+\cos\phi)$. The κ_x complex plane is mapped into the complex α-plane shown in Fig. 3(b). The poles $\kappa_{xi}^{\mathrm{GW}}$ are mapped into the poles $\alpha_i^{\mathrm{GW}}(G = L, S)$. A couple of OP's are located at $\alpha = \pm(\pi-\phi)$ (the pole at $\pi-\phi$ corresponds to the OP on the top Rieman sheet of the κ_x plane). The integration contours $C_\alpha \equiv (-j\infty, \pi + j\infty)$ maps axis of the κ_x-plane; it detours the imaginary poles α_i^{SW} in the clockwise and counterclockwise sense for the portion $(-j\infty, 0)$ and $(\pi, \pi+j\infty)$, respectively. The OP located in $[-\pi,\ \pi]$ is always detoured in counterclockwise sense.

To evaluate asymptotically the integral in (4) for large kL, the integration contour is deformed into the SDP through its pertinent saddle point of the integrand at $\alpha = 0$. This deformation is allowed only for $L > h$, because $A(\alpha)$ behaves like $\exp(jkh\cos\alpha)$ for large positive value of the immaginary part of α. In this deformation, OP's, SW poles, or LW poles may be captured and their residue accounted for, thus leading to

$$a(\phi) + e^{jkL\cos\phi} = a^{\mathrm{go}} + a^d + \sum_n a_n^{\mathrm{SW},d} + \sum_m a_m^{\mathrm{LW},d} \tag{5}$$

where a^d is defined as in (4), but with integration on the SDP; and the other terms derive from the residue contributions (for homogeneity of notation, the term $\exp(jkL\cos\phi)$ associated to the incident field is incorporated in the contribution a^{go}, denoting the GO field)

$$a^{\mathrm{go}} = e^{jkL\cos\phi}[1 + r_+^{\mathrm{go}} U(\pi-\phi) + r_-^{\mathrm{go}} U(-(\pi-\phi))] \tag{6}$$

$$a_n^{\mathrm{SW},d} = r_n^{\mathrm{SW}} e^{jkL\cos\alpha_n^{\mathrm{SW}}} U\left(-\mathrm{Im}\left(\alpha_n^{\mathrm{SW}}\right)\right) \tag{7}$$

and (8), shown at the bottom of the page, where $r_\pm^{\mathrm{go}}$ is the residue of $A(\alpha)$ at $\pm(\pi-\phi)$ and r_i^{GW} is the residue of $A(\alpha)$ at $\alpha_i^{\mathrm{GW}}(G = S, L)$. Moreover, $U(\eta)$ is the heavyside unit step functions ($U = 1$ for $\eta > 0$ and $U = 0$ for $\eta < 0$), and in (8), $\mathrm{Re}(\alpha_m^{\mathrm{GW}}) \in [0, \pi/2)$.

By inspection of the phase terms, the various contributions in (6)–(8) can be interpreted in terms of rays, which are those schematized in Fig. 2.

In the upper half-space $(\phi < \pi)$ a^{go} is the GO (space-wave) contribution. It consists of the contribution from the source field modulated by the presence of the infinite grounded slab as presented in Fig. 2(a). In Appendix A, it is demonstrated that $r_-^{\mathrm{go}} = -1$, so that (6) implies a^{go} vanishes in the lower half-space $(\phi > \pi)$. This is expected since for the infinite slab the radiation of the ground and volumetric currents must cancel the contribution from the unit line source. A compact expression of this contribution is

$$a^{\mathrm{go}} = U(\pi-\phi)p(\phi)e^{jkL\cos\phi} \tag{9}$$

where $p(\phi)$ is given in Appendix A, (21). Note that $p(\phi)$ vanishes at the limit $\phi \to \pi^-$ as anticipated in Section II-A; thus, only a slope-type contribution of space-wave diffraction is expected.

The phase-exponential factor in (7) and (8) leads to interpret a_m^{SW} and a_n^{LW} as the diffraction contribution of the SW's and LW's excited into the slab [see Figs. 2(b) and (c), respectively]. The SW diffraction gives the most significant contribution, particularly at grazing aspects. As mentioned earlier, the LW-induced diffraction is negligible in most cases. Note that the SW and LW direct field contribution do not appear in the far zone representation (5), being exponentially attenuated along y.

The term a^d can be interpreted as the diffraction contribution of the space wave. As mentioned in Section II-A, this contribution is intended to provide the required uniform continuity to the GO field when the observation point approaches $\phi = \pi$ and also a uniform description of the SW and LW excitation phenomena when a frequency variation occur around the cutoff. The asymptotic evaluation of a^d is performed next.

Before proceeding further, we note that $A(\alpha)$ and the relevant derived quantities can be decomposed in the two terms associated to the first and second term of Appendix A, (18); since the second term of such an equation exhibits a phase factor $\exp(-jkh\sin\phi)$, all the diffracted ray deriving from it can be interpreted as coming from the the lower edge of the truncation (see Fig. 2).

B. Asymptotic Evaluation of the Space Wave Diffracted Field

The asymptotic evaluation of the SDP integral which defines the space-wave diffracted field is performed via the Van der Waerden (VdW) method [7], [13]. The asymptotic evaluation is dominated by the saddle-point contribution, but is sensitive to whether the poles is near the SDP and/or are crossed by the SDP. If the pole and the SDP are distinct, each can be evaluated separately from the other. When the SDP and pole are contiguous, the asymptotics must be refined, i.e., made uniform, to account simultaneously for both. Note that the L/SW poles and the OP migrate in the complex plane depending on different parameters, that is, on the observation angle and on the frequency (slab thickness and permittivity being fixed), respectively. In particular, the OP approaches the saddle point when the observer approaches the grazing aspect $(\phi = \pi)$, while the SW poles do the same when the frequency is close to the relevant cutoff frequency that defines the excitation condition of each SW. The

$$a_m^{\mathrm{LW},d} = r_m^{\mathrm{LW}} e^{jkL\Re e(\kappa_{xm}^{\mathrm{LW}})} e^{-kL\Im m(\kappa_{xm}^{\mathrm{LW}})} U\left(\frac{1}{\cosh(\mathrm{Im}\,(\alpha_m^{\mathrm{LW}}))} - \cos\left(\mathrm{Re}\,\alpha_m^{\mathrm{LW}}\right)\right) \tag{8}$$

VdW procedure for the present case is as follows. After substituting $\cos\alpha = 1 - js^2$ in the α integral, the term $A(\alpha)$ in the integrand is transformed into $B(s) = -J(1-js^2, \phi)2s/(s^2 - s_o^2)$, where $s_o = \sqrt{2/j}\cos((1/2)\phi)$, while the SDP contour transforms in the real axis of the s plane. Each pole of $B(s)$ is individually extracted from the spectral integrand

$$B(s) = \frac{r_+^{\mathrm{go}}}{s - s_0} + \frac{r_-^{\mathrm{go}}}{s + s_0} + \sum_i \frac{r_i^{\mathrm{GW}}}{s - s_i^{\mathrm{GW}}} + T(s) \qquad (10)$$

thereby isolating the pole contribution from the resulting regularizing remainder $T(s)$. In (10), $s_i^{\mathrm{GW}} = \sqrt{2/j}\sin((1/2)(\alpha_i^{\mathrm{GW}}))(G = S, L)$ where α_i^{GW} are both LW and SW poles in the complex plane that possesses real part between $-\pi/2$ and $\pi/2$ [see Fig. 2(b)]. The regular function $T(s)$ is then approximated by the first two terms of its Taylor expansions at the saddle point. Finally, a term-by-term closed-form integration is carried out, thus leading to (11), shown at the bottom of the page, where $F(y)$ is the transition function of the Uniform Theory of Diffraction (UTD), defined with $-3\pi/4 < \arg(\sqrt{y}) \le \pi/4$ (see [8, eq. (41b)]); $r_i^{\mathrm{SW}}, r_i^{\mathrm{LW}}$ and $p(\phi)$ are the same as that introduced in (7), (8), and (9), respectively. The summation in (11) includes the LW and SW poles close to the saddle point $(s = 0)$ and not necessarily correspond to those captured in the SDP deformation. Each term of the i-indexed sum in (11) provide a uniform description of the field when the frequency crosses the cutoff frequency of the associate SW or LW (i.e., when a SW or a LW pole crosses the SDP). Furthermore, $T(0)$ and $T''(0)$ (the second derivative of $T(s)$ at $s = 0$) are easily obtained from (10). By using their explicit expressions, which can be easily obtained setting $s = 0$ in (10), (11) can be rearranged as (12), shown at the bottom of the page, where $\Im(x) = 1 - F(x) - 1/(2jx)$ is such that $\Im(x) \sim (3/4)x^{-2}$ for x large. The explicit expression of $B''(0)$ is given in Appendix A. Equation (12) highlights well the slope nature of the space-wave diffracted ray. Indeed, for large kL and far from transitions (i.e., far from $\phi = 0$ and far from the cutoff frequency of surface waves) the asymptotic dominant term is that relevant to $B''(0)$, which is of order $(kL)^{-3/2}$ (since $\Im(x) \sim (3/4)x^{-2}$). This agrees with the anticipated $x^{-3/2}$ spreading of the grazing space-wave (see Section II-A).

IV. Integral Equation and MoM Solution

In order to provide a reference solution for the problem in Fig. 1, an integral equation is formulated and then solved via a method of moments (MoM). Due to the infinite extent of the structure, the surface for defining equivalent unknown currents must be infinite, thus requiring basis functions which extent to infinity. For penetrable objects of finite extension, the continuity of the tangential fields is usually applied to the external profile of the object itself. For the present infinite configuration, this conventional approach may cause difficulties. Indeed, when the SW's are excited, undamped unknown currents need to be distributed along the x direction, thus implying truncation errors or, when using entire domain basis functions, yielding poor convergence of the reaction integrals. Although these latter difficulties may be overcome by using the method described in [14], close to the excitation condition of surface waves still remain open problems. In order to avoid the above difficulties, we enforce the tangential field continuity across the aperture surface S coincident with the y-z plane; indeed, on this surface, the SW's are exponentially attenuated so that the asymptotic field is only due to the GO and to the space-wave diffracted contributions that exhibit a known asymptotic behavior. The surface S is the same as that used in [15] for estimating the surface wave PO diffraction at the edge of an impedance half-plane.

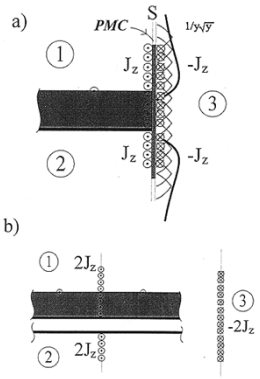

Fig. 4. (a) Application of the equivalence principle to the actual problem. On the surface S, the profile of the basis functions used in the MoM are depicted. (b) Equivalent problems for the regions 1, 2, and 3 obtained by applying the image principle.

The surface S divides the space in three regions, denoted by 1) $(x > 0, y > -h)$; 2) $(x > 0, y < -h)$; and 3) $(x < 0)$, respectively [Fig. 4(a)]. By invoking the equivalence principle at S electric and magnetic equivalent unknown currents are distributed on the two sheets $x = 0^+$ and $x = 0^-$, which are infinitely close to the surface $x = 0$. Next, an infinitesimally thin perfectly magnetic conductor (PMC) is placed between these sheets so that the magnetic currents do not radiate and can be suppressed. As a consequence, the problem is purely TM with

$$a^d \sim \frac{e^{-jkL}}{2j\sqrt{\pi kL}} \left\{ p(\phi)\frac{F\left(jkLs_0^2\right)}{s_0} + \sum_i r_i^{\mathrm{GW}} \frac{F\left(jkL\left(s_i^{\mathrm{SW}}\right)^2\right)}{s_i^{\mathrm{GW}}} - \left[T(0) + \frac{T''(0)}{4kL}\right] \right\} \qquad (11)$$

$$a^d \sim \frac{e^{-jkL}}{2j\sqrt{\pi kL}} \left\{ p(\phi)\frac{\Im\left(jkLs_o^2\right)}{s_0} + \sum_i r_i^{\mathrm{GW}} \frac{\Im\left(jkL\left(s_i^{\mathrm{GW}}\right)^2\right)}{s_i^{\mathrm{GW}}} - \frac{B''(0)}{4kL} \right\} \qquad (12)$$

respect to z and the electric current on the aperture are directed along z and denoted by $J_z^{\pm}$ for $x = 0^{\pm}$. The continuity of the tangential magnetic field implies that these electric currents have equal amplitudes and opposite signs on the two sides of the surface S [i.e., $J_z^+ = -J_z^- = J_z$, Fig. 4(a)]. The continuity of the tangential electric field is then enforced to obtain the integral equation

$$\left[E_z^i + E_z(J_z)\right]_{x=0^+} = E^z(-J_z)|_{x=0^-} \tag{13}$$

where E_z^i is the z-directed field of the impressed line source and $E_z(\pm J_z)$ is the z-directed field radiated by $\pm J_z$ in the proper region. By applying the image principle, the field in each region can be calculated by using the equivalent problems depicted in Fig. 4(b). Each one of them can be treated by using standard Green's functions; in particular, in region 1, the problem reduces to an infinite grounded slab illuminated by two line sources placed at symmetric distances from S and from $2J_z(y > -h)$ implying the use of the Green's function of the infinite slab. In regions 2 and 3, the problems reduce to sheets of currents radiating in free-space.

The unknown equivalent electric current J_z is expanded in terms of basis functions $J_n(y)(n = 0, N)$ weighted by unknown coeficients I_n to be determined via a MoM scheme. In particular, for $n = 1, N-1$, symmetric piecewise sinusoidal (PWS) basis functions are used to cover the portion of S near $y = 0$ [Fig. 4(a)]. The first N_0 PWS are those for $y > 0$ ($n = N_0$ corresponds to that with its maximum at the origin). Moreover, two additional entire domain basis functions (EDBF's) are used for describing the far-out region of the aperture. The appropriate asymptotic behavior of the EDBF's can be deduced by observing that in the far zone, the dominant contribution of the magnetic field on the aperture must be directed along x. This means that the magnetic field component along y, which is responsible for the electric currents along z, possesses a $\exp(-jky)/y\sqrt{y}$ asymptotic behavior. This occurs for both the space-wave field and the diffracted rays excited by all the slab-modulated incident waves. Then, the EDBF's are expressed via their spectral Fourier representation as $J_0(y) = f(y)$ and $J_N(y) = f(-y-h)$, where

$$f(y) = \frac{\sqrt{k}}{2\pi}\int_{-\infty}^{\infty} \frac{e^{-jk_y y}}{\left(\sqrt{k-k_y}+\sqrt{k-K}\right)^3} dk_y \tag{14}$$

in which $K = kh/\sqrt{h^2+L^2}$ and the branch cut is defined so as $\arg(\sqrt{k-k_y}) \in (-\pi/4, 3\pi/4)$ in the top Riemann sheet; the integration contour detours the branch point $k_y = k$ in a clockwise sense. It can be demonstrated that (14) exhibits the expected $\exp(-jky)/(y\sqrt{y})$ asymptotic behavior. Moreover, Jordan's lemma shows that $f(y)$ vanishes for $y \le 0$; as a consequence, $J_0(y)$ and $J_N(y)$ are dropped to zero and $-h$, respectively. It is worth noting that the complex constant K may be chosen with a certain degree of freedom to regulate the distance at which $f(y)$ reaches the asymptotic regime. However, its value has a little influence on the convergence rate of the MoM solution.

The MoM solution of the integral equation is obtained by using PWS weighting functions. The reaction integrals, which define the mutual impedance and the forcing term, are calculated in the spectral domain for all the three regions. Since regions 2 and 3 involve ordinary free-space Green's function, their calculation is straightforward. In region 1, which involves the infinite slab Green's function, the strategy for the calculation of the reaction integral is described in Appendix B.

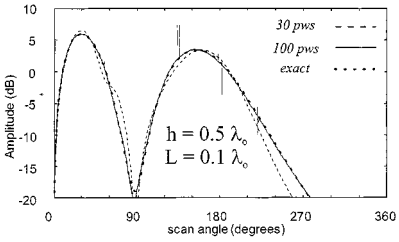

Fig. 5. Far field of a line source placed on a half-plane with $\rho = 50\lambda_0$, $L = 0.1\lambda_0$ and $h = 0.5\lambda_0$. Exact solution (marks); MoM solution $N = 30$ (dashed line); MoM solution $N = 100$ (continuous line).

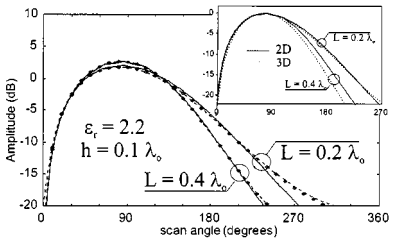

Fig. 6. Normalized far field for thin grounded slab ($h = 0.1.\lambda$) with $\epsilon_r = 2.2$ for two different positions of the source ($L = 0.2\lambda$ and $L = 0.1\lambda$). MoM solution (continuous line); PO numerical integration (marks); PO asymptotic solution (dashed line). In the inset: comparison between the normalized field from a line source illumination [two-dimensional (2-D), continuous line] and from a dipole illumination (3-D), dotted line].

V. Numerical Results

In this section, comparison between PO and MoM results will be presented, with an objective to find the range of validity of the PO approximation. The plots in Figs. 6–10 represent the E_z field in the far zone normalized with respect to the same far-field component radiated by an electric line source in free-space; for the PO formulation presented here, this corresponds to the pattern $a(\phi) + \exp(jkL\cos\phi)$ in (1). For the MoM solution, PWS with $d/2 = 0.05\lambda_0$ is used.

In order to validate the numerical procedure, a preliminary example is presented for the case $\epsilon_r = 1$, which corresponds to a line source above a perfectly electric conducting half-plane (Fig. 5). For this case, the available exact solution has been compared with the MoM results. In particular, the field at distance $\rho = 50\lambda_0$ for $L = 0.1\lambda_0$ and $h = 0.5\lambda_0$ is calculated by our technique using two different number of PWS. The curve of the exact solution almost superimposes to that from MoM for the case $N = 100$ ($N_0 = 75$). Using the above geometry for different values of L and h allowed us to calibrate the number of PWS to be used; for L and h less than $0.5\lambda_0$, no more than 100 are needed.

In Figs. 6–9, the PO results are obtained from (5) by calculating the space-wave diffracted field contribution a^d both via numerical integration on the SDP (marks) and via the asymptotic expression (11) (dashed line). The MoM results are always

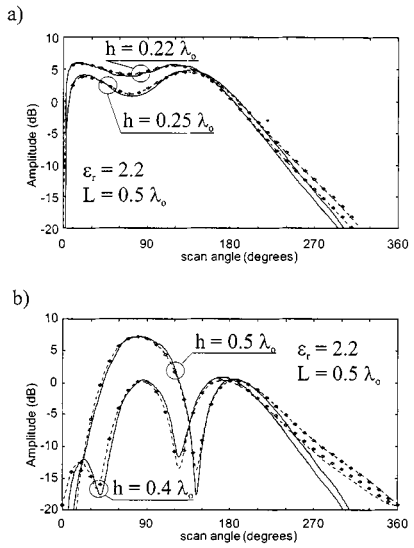

Fig. 7. Normalized far-field pattern for a source at $L = 0.5\lambda_0$ from the edge for various thicknesses of a slab with $\epsilon_r = 2.2$; the cutoff frequency of the TE_y mode occurs for $h = 0.28\lambda_0$. MoM solution (continuous line); PO numerical integration (marks); PO asymptotic solution (dashed line). (a) $h = 0.22\lambda_0$, $h = 0.25\lambda_0$. (b) $h = 0.40\lambda_0$, $h = 0.50\lambda_0$.

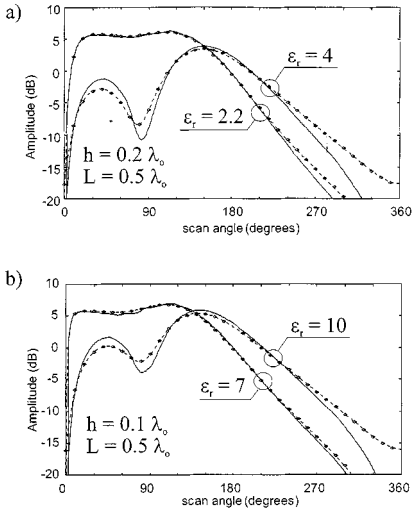

Fig. 8. Normalized far-field pattern for a source at $L = 0.5\lambda_0$ from the edge for various permittivities and thicknesses of the slab. MoM solution (continuous line); PO numerical integration (marks); PO asymptotic solution (dashed line). (a) $h = 0.2\lambda_0$, $\epsilon_r = 2.2$, $\epsilon_r = 4$. (b) $h = 0.1\lambda_0$, $\epsilon_r = 7$, $\epsilon_r = 10$.

presented by a continuous line. In all the cases, the curves of the numerical PO calculation and its relevant asymptotics are almost superimposed, thus demonstrating the robustness of the asymptotic solution also for moderate values of kL.

Fig. 6 shows the effectiveness of the PO approximation for a small thickness of the substrate $(h = 0.1\lambda_0)$, for a low dielectric constant $(\epsilon_r = 2.2)$, and for small distances between the source and the edge $(L = 0.2\lambda_0$ and $0.4\lambda_0)$. In the inset of Fig. 6, the same results are compared with those obtained by using the formulation in [7], which is based on the same PO approach, but using an elementary dipole as a source. This allows to evaluate how close this 2-D formulation is to the correspondent 3-D

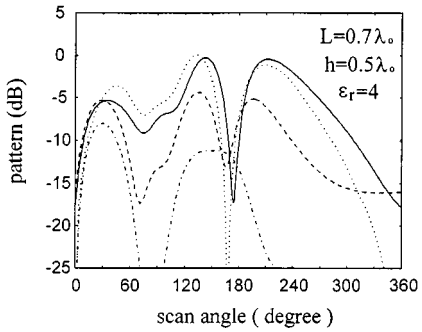

Fig. 9. Normalized far-field pattern for $L = 0.7\lambda_0$ with $h = 0.5\lambda_0$ and $\epsilon_r = 4$. Two SW's are excited: SW_1(with lower cutoff frequency $f_1 = c/(4h\sqrt{\epsilon_r - 1})$) and SW_2 (with higher cutoff frequency $f_2 = 3c/(4h\sqrt{\epsilon_r - 1})$). MoM solution (dotted line); PO asymptotic solution (continuous line); PO without SW_2 diffraction (dashed line); PO without SW_2, and SW_1 diffraction (dash-dotted line).

formulation (unless in the *H*-plane, where the diffraction contribution of the dominant TM SW is weaker). We emphasize again that the application of the 3-D formulation to patch antenna problems on a finite rectangular substrate is presented in [8].

The same dielectric constant $(\epsilon_r = 2.2)$ as that in Fig. 6, with a different source location $(L = 0.5\lambda_0)$ is considered in Fig. 7 for increasing substrate thicknesses in terms of a wavelength. In particular, Fig. 7(a) presents two slightly different situations: $h = 0.22\lambda_0$ and $h = 0.25\lambda_0$, which correspond to whether or not the first SW is excited (the cutoff frequency occurs for $h = 0.228\lambda_0$). This example is intended to check the validity of the asymptotic PO solution inside the transition of the space wave diffracted field, which must ensure continuity to the SW diffraction contribution [this corresponds to a SW pole crossing the saddle point, see Fig. 3(b)]. When the thickness further increases [$h = 0.4\lambda_0, 0.5\lambda_0$, Fig. 7(b)], the SW diffraction contribution gradually assumes relevance, observable by the presence of a second radiation lobe close to the paraxial direction $(\phi = 180°)$. The agreement between PO and MoM results is excellent for the cases of Fig. 8(a) and satisfactory for those of Fig. 7(b). In the latter cases, the curves corresponding to PO and MoM start to deviate one from the other at 220°; this may be attributed to the inability of PO in recovering the boundary conditions of the perfectly conducting ground plane (vanishing E_z-field for $\phi = 360°$).

The example in Fig. 8 shows the efficacy of PO in describing cases with high values of dielectric constants. Two different thicknesses are chosen ($h = 0.2\lambda_0$, Fig. 8(a), and $h = 0.1\lambda_0$, Fig. 9(b)); for each of them two permittivities are considered [$\epsilon_r = 2.2, \epsilon_r = 4$, Fig. 8(a); $\epsilon_r = 7, \epsilon_r = 10$, Fig. 8(b)]. For each pair, the lower and higher ϵ_r correspond to SW below or above the cutoff, respectively. Note that the paraxial lobe due to the SW diffraction is dominant in both the cases when the SW's are excited and more pronounced than that in Fig. 7(b) due to the larger amplitude of the SW excitation coefficient. The agreement is again satisfactory, but a discrepancy occurs in the region from 45° to 90°. This may be attributed to a nonnegligible diffraction contribution from the edge excited SW traveling backward, which is neglected in the PO approach.

Fig. 9 corresponds to $L = 0.7\lambda_0, h = 0.5\lambda_0$ and $\epsilon_r = 4$. For this case, two SW's are excited in the dielectric. We denote by SW_1 and SW_2, the one having lower (higher) cutoff frequency, respectively. Furthermore, a LW is excited in this case. The MoM result (dotted line) is compared with that from the asymptotic PO (numerical evaluation of PO is not reported here, because it gives a curve superimposed with the asymptotics). In order to appreciate the nature of the SW diffracted field contribution, two other curves are depicted that correspond to the total field without the diffraction contribution of SW_2 (dashed line) and without both SW_1 and SW_2 (dash-dotted line). The LW diffracted field is not depicted in this figure because it has negligible effect on the pattern. Unlike previous results, the PO curve slightly deviates from that from MoM in the broadside region; this may again be attributed to the inability of PO in describing the diffraction contribution from the SW's reflected at the truncation. Comparisons with the other curves shows that the diffraction contribution of the SW's (especially that of SW_1) dominates the total field starting from $\phi = 45°$.

VI. Concluding Remarks

The effectiveness of the PO approximation has been demonstrated in describing diffraction effects of the various wave species excited by a line source in a truncated slab problem. To avoid the presence of multiple diffraction effects that could have confused the interpretation of the mechanisms arising by a single truncation, a semi-infinite slab instead of a finite one has been chosen as a validation problem. An asymptotic solution is given for the PO in the far-field region, which is successfully validated against PO numerical integration also for moderate values of the asymptotic parameter L, which is the distance of the source from the upper edge. The PO results have been compared with those from a full-wave analysis, which is carried out by solving via a MoM scheme an IE expressing the continuity of the tangential electric field on an infinite aperture orthogonal to the slab. This approach, although rather unconventional, led to stable convergence properties and numerical efficiency, reducing the required number of unknowns. The latter is obtained by using EDBF's that are shaped in such a way to reconstruct the asymptotic aperture field.

Comparisons with the MoM solution has shown the following expected limitations of the PO formulation.

1) PO is not accurate in predicting the far-field pattern close to $\phi = 360°$. This is attributed to the failing to meet the boundary condition of the perfectly electric conducting ground plane. This limitation can be overcome by adding to the PO field a fringe field contribution arising from the diffracted currents on the perfectly conducting plane. The formulation of this contribution is presently under investigation.
2) When the slab is electromagnetically dense and thick in terms of a wavelength so that the SW reflected back at the truncation produce significant end-point radiation, the present PO formulation fails. On the basis of a wide set of examples it is deduced that this occurrence arises in practice when the first two guided modes are excited into the slab (i.e., for the present TE_y case for $h = (3/4)\lambda_0/\sqrt{\epsilon_r - 1}$). This can be considered as an approximate limit for the applicability of PO.

Appendix A

The expressions of the PO current in the spectral domain is

$$J_z^{\mathrm{PO}}(\kappa_x, y) = \frac{k(\epsilon_r - 1)\sin[hk(y+h)\kappa_{y1}] - \kappa_{y1}\delta(y+h)}{\mathrm{TE}(\kappa_y, \kappa_{y1})} \tag{15}$$

where δ is the Dirac's delta function and

$$\mathrm{TE}(\kappa_y, \kappa_{y1}) = \kappa_{y1}\cos(hk\kappa_{y1}) + j\kappa_y \sin(hk\kappa_{y1}) \tag{16}$$

with $\kappa_y = \sqrt{1 - \kappa_x^2}, \kappa_{y1} = \sqrt{\epsilon_r - \kappa_x^2}$. The first and second term corresponds to the polarization and the surface ground currents, respectively.

Using (17), shown at the bottom of the page, a closed-form expression for $J(\kappa_x, \phi) = \int_{-h}^{0} J_z^{\mathrm{PO}}(\kappa_x, y)\exp(jky\sin\phi)\,dy$ is obtained [see (18), at the bottom of the page]. Denote by $J_0(\kappa_x, \phi)$ and $J_1(\kappa_x, \phi)$ the first and second term of (18). When $\kappa_x = -\cos\phi, \kappa_y = -\sin\phi$ (this corresponds in the α-plane to the optical pole $\phi - \pi$ *which is captured by the deformation contour for* $\phi < \pi$), we have (19), shown at the bottom of the page, with $t = \sqrt{\epsilon_r - \cos^2\phi}$. From (19), we obtain

$$p(\phi) = \frac{2j\sin\phi\sin(hkt)}{t\cos(hkt) + j\sin\phi\sin(hkt)} \tag{20}$$

$$k\int_h^0 \sin[\kappa_{y1}(y+h)]e^{jk(y+h)\sin\phi}\,dy = \frac{\kappa_{y1} - e^{jkh\sin\phi}\mathrm{TE}(-\sin\phi, \kappa_{y1})}{(\kappa_{y1}^2 - \sin^2\phi)} = I(\kappa_x, \phi) \tag{17}$$

$$J(\kappa_x, \phi) = \frac{-(\epsilon_r - 1)\mathrm{TE}(-\sin\phi, \kappa_{y1})}{(\kappa_{y1}^2 - \sin^2\phi)\,\mathrm{TE}(\kappa_y, \kappa_{y1})} + \kappa_{y1}\frac{\epsilon_r - 1 - \kappa_{y1}^2 + \sin^2\phi}{(\kappa_{y1}^2 - \sin^2\phi)\,\mathrm{TE}(\kappa_y, \kappa_{y1})}e^{-jkh\sin\phi} \tag{18}$$

$$J_o(-\cos\phi, \phi) = -\mathrm{TE}(-\sin\phi, t)/\mathrm{TE}(\sin\phi, t) \quad \text{and} \quad J_1(-\cos\phi, \phi) = 0 \tag{19}$$

$$B''(0) = \frac{-2\sqrt{2j}\sin(kh\sqrt{\epsilon_r - 1})\exp(-jkh\sin\phi)}{\cos^2(\frac{1}{2}\phi)\cos^2(kh\sqrt{\epsilon_r - 1})}\left(I(1,\phi) - \frac{1}{\sqrt{\epsilon_r - 1}}\right) \tag{22}$$

in (9). For $\kappa_x = -\cos\phi$, $\kappa_y = \sin\phi$ (this corresponds in the α-plane to the optical pole $\phi - \pi$ *which is captured by the deformation contour for* $\phi > \pi$) we obtain

$$J_o(-\cos\phi, \phi) = -1; \quad J_1(-\cos\phi, \phi) = 0. \tag{21}$$

This latter expression is also valid for the improper pole (i.e., the one not captured) when $\phi < \pi$. Thus, one can easily conclude that $r_{-}^{\text{go}} = -1$. The explicit expression of $B''(0)$ in (12) is (22), shown at the top of the page, where $I(\kappa_x, \phi)$ is defined in (17).

APPENDIX B

The spatial slab Green's function (GF) $g(y, y')$ pertinent to a line source placed at $(x = 0, y')$ with observer at $(x = 0, y)$ is represented via the y transmission-line formalism ([15], chapter 5)

$$g(y, y') = \int_{-\infty}^{\infty} G(k_x, y, y')\, dk_x \tag{23}$$

where the branch cuts are conveniently defined by $\text{Im}\sqrt{k^2 - k_x^2} = 0$, being $\text{Im}\sqrt{k^2 - k_x^2} < 0$ the principal Riemann sheet. Two different cases are distinguished that are relevant to nonoverlapped and overlapped PWS's functions.

1) The reaction integrals involving nonoverlapped basis functions are performed in the spectral domain directly in the κ_x variable. Since the spacing $s = |y_i - y_j|$ in between the phase centers y_i and y_j of the PWS's is greater than their domain d, the term $\exp(-j(s-d)\sqrt{k^2 - k_x^2})$ in the integrand is attenuating for large k_x, thus ensuring good convergence properties. To avoid the presence of poles along the integration path, a deformation is performed along the contour defined by the equation $k_{xi} = k_{xr}\exp(-k_{xr}^2/(2k^2))$ being $k_x = k_{xr} + jk_{xi}$. No poles are never captured in this contour deformation.
2) The reaction integrals involving overlapped basis functions are performed in the spectral domain by using the change of variable $k_y = \sqrt{k^2 - k_x^2}$. To this end, the integral in (45) is rewritten in terms of the y-transformed spectral variable k_y (with $\text{Im}\sqrt{k^2 - k_y^2} < 0$ on the principal Riemann sheet). The contour in the k_y plane, which corresponds to the real k_x axis, runs along the branch-cut $\text{Im}\sqrt{k^2 - k_y^2} = 0$. For the sake of convenience, it is deformed along the real axis by including the pertinent residues of SW and LW poles. This approach has been preferred to the one described above since it does not require to break up the various exponential terms of the PWS's spectra, which is necessary for ensuring convergency of the direct k_x integration for $s < d$. This approach has also been used to evaluate the reaction integrals involving EDBF's.

REFERENCES

[1] E. Lier and K. R. Jacobsen, "Rectangular microstrip antennas with infinite and finite ground plane dimensions," *IEEE Trans. Antennas Propagat.*, vol. AP-31, pp. 978–984, 1983.

[2] J. Huang, "Finite ground plane effects on microstrip antennas radiation patterns," *IEEE Trans. Antennas Propagat.*, vol. AP-31, pp. 649–653, 1983.

[3] S. A. Bokhari, J. R. Mosig, and F. E. Gardiol, "Radiation pattern computation of microstrip antennas on finite size ground plane," *Proc. Inst. Elect. Eng.— Pt. H*, vol. 139, no. 3, pp. 278–286, 1992.

[4] O. M. Bucci and G. Franceschetti, "Electromagnetic scattering by a half plane with two face impedances," *Radio Sci.*, vol. 11, pp. 49–59, Jan. 1976.

[5] R. G. Rojas, "Electromagnetic diffraction of an obliquely incident plane wave field by a wedge with impedance faces," *IEEE Trans. Antennas Propagat.*, vol. 36, no. 7, pp. 956–970, July 1988.

[6] H. C. Ly, G. Rojas, and P. H. Pathak, "EM plane wave diffraction by a planar junction of two thin material half-plane—Oblique incidence," *IEEE Trans. Antennas Propagat.*, vol. 41, no. 4, pp. 429–441, 1993.

[7] S. Maci, L. Borselli, and L. Rossi, "Diffraction at the edge of a truncated grounded dielectric slab," *IEEE Trans. Antennas Propagat.*, vol. 44, pp. 863–873, June 1996.

[8] L. Borselli and S. Maci, "Asymptotic, closed-form expressions for the field radiated by a patch on a finite substrate," *J. Electromagn. Wave Applicat.*, vol. 11, pp. 689–711, June 1997.

[9] T. K. Sarkar and E. Arvas, "An integral equation approach to the analysis of finite microstrip antennas: Volume/surface formulation," *IEEE Trans. Antennas Propagat.*, vol. 38, pp. 305–312, Mar. 1990.

[10] J. A. Kong, *Electromagnetic Wave Theory*, New York: Wiley, 1986, pp. 325–328.

[11] S. Maci, S. Raffaelli, M. Leoncini, L. Borselli, and P.-S. Kildal, "Analysis of SW excitation and radiation mechanisms of a monopole on a circular grounded dielectric slab with critical thickness," *Proc. Inst. Elect. Eng. — Pt. H*, vol. 143, no. 4, pp. 335–340, Aug. 1996.

[12] D. R. Jackson and A. A. Oliner, "A leaky-wave analysis of the high-gain printed antenna configuration," *IEEE Trans. Antennas Propagat.*, vol. 36, pp. 905–910, July 1988.

[13] V. L. Van der Waerden, "On the method of saddle points," *Appl. Sci. Res.*, vol. B2, pp. 33–45, 1951.

[14] L. S. Andersen, O. Breinbjerg, and J. T. Moore, "The standard impedance boundary condition model for coated conductors with edges: A numerical investigation of the accuracy for transverse magnetic polarization," *J. Electromagn. Wave Applicat.*, vol. 12, pp. 415–446, May 1998.

[15] L. B. Felsen and N. Marcuvitz, *Radiation and Scattering of Waves*. New York: Prentice-Hall, 1973, p. 565.

Stefano Maci (M'92–SM'99) was born in Rome, Italy, in 1961. He received the Ph.D. degree in electronic engineering from the University of Florence, Italy, in 1987.

In 1990, he joined the Department of Electronic Engineering of the University of Florence, Italy, as an Assistant Professor. Since 1998 he has been an Associate Professor at the University of Siena, Italy. In 1997 he was an Invited Professor at the Technical University of Denmark, Copenhagen. Since 1996 he was involved in projects of the European Space Agency regarding the electromagnetic modeling of antennas. His research interests are focused on electromagnetic theory, mainly concerning high-frequency methods for electromagnetic scattering and diffraction. He also developed research activity on microwave antennas, with a particular focus on the analysis, synthesis, and design of patch antennas.

Dr. Maci received the National Young Scientists "Francini" award for the Laurea thesis in 1988 and the "Barzilai" prize for the Best Paper at the National Italian Congress of Electromagnetism (XI RiNEm) in 1996. He is an associate editor of the IEEE TRANSACTIONS ON ELECTROMAGNETIC COMPATIBILITY.

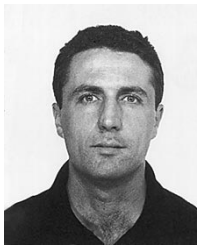

Leonardo Borselli (M'95) was born in Florence, Italy, in 1966. He received the Laurea (*cum laude*) (electronic engineering) and Ph.D. (electromagnetism) degrees from the University of Florence, Italy, in 1992 and 1996, respectively.

From 1996 to 1998, he was involved in a Postdoctoral program at the University of Siena, Italy, where now he is working as a Teacher of electromagnetic fields at the Diploma di Laurea. His research interests are mainly concerned with theoretical and applied electromagnetics, particularly with high-frequency methods for electromagnetic scattering, numerical methods, and printed antennas.

Andrea Cucurachi was born in Thiene, Italy, in 1971. In 1998, he received the Laurea degree (*cum laude*) in telecommunication engineering.

In 1997, he obtained a fellowship at MoTheSim, Les Plessis Robinson, France, where he was involved in research activity on radar polarimetry. He is currently a Designer of radio links at the R&D Department, Italtel, Milano, Italy. His research activity is mainly concerned with scattering from rough surfaces and applications of the geometrical theory of diffraction.